Theoretical and Applied Fracture Mechanics 107 (2020) 102490

Contents lists available at ScienceDirect

Theoretical and Applied Fracture Mechanics

journal homepage: www.elsevier.com/locate/tafmec

Elastoplastic 3D analyses of plastic zone size dependencies on load-to-yield strength and on crack size-to-width ratios under mixed mode I/II

Luiz Fernando Nazaré Marques[a,*], Marco Antonio Meggiolaro[b], Jaime Tupiassú Pinho de Castro[b], Luiz Fernando Martha[b]

[a] Federal University of South and Southeast of Pará, UNIFESSPA, Avenida dos Ipês s/n, Marabá 68500-000, Brazil
[b] Pontifical Catholic University of Rio de Janeiro, PUC-Rio, Rua Marquês de São Vicente 225, Rio de Janeiro 22451-900, Brazil

ARTICLE INFO

Keywords:
Mixed-mode K_I-K_{II}
3D finite elements
Incremental elastoplastic calculations
Plastic zone estimates
Elastoplastic work

ABSTRACT

A pure mode-I approach cannot properly analyze many important practical problems that involve combined mode I and II loadings, which in particular may not be sufficient to estimate crack paths and fracture toughness in such cases. Multiaxial crack tip conditions characterized by a crack inclination angle β in a modified mixed-mode single edge tension SE(T) specimen are used to consider mixed-mode effects on the shapes and volumes of the plastic zones (*pz*) that form ahead of crack tips, as well as on the plastic work U_{pl} dissipated inside them. A methodology is proposed to evaluate *pz* volumes V_{pz} based on a sub-modeling FE analysis that uses the influence volume around a plastified Gauss integration point. For a given Equivalent Stress Intensity Factor K_{eq}, both V_{pz} and U_{pl} are evaluated for different nominal stress to yield strength ratios σ_n/S_Y and several combinations of geometric parameters β, W/B and a/W, where a is the crack size, W is the cracked specimen width, and B is its thickness. Before performing all these analyses, compatibility and convergence studies are carried out to validate the submodels used in such analyses.

1. Introduction

Elastoplastic (EP) stress/strain fields around crack tips are most important in structural integrity evaluations. Damage accumulated in them is the actual driving force for failure mechanisms such as fatigue crack growth (FCG), stable crack tearing, unstable fracture, and even environmentally assisted cracking. Since cracks prefer to grow perpendicular to the main principal stress (at least when it is tensile), most engineering problems that involve FCG and fracture can be properly modeled by taking into account only mode-I features. However, there are many important problems where the combined effect of mixed mode I and II loadings cannot be neglected. In particular, a pure mode-I approach may not be sufficient to estimate, for practical purposes, fracture toughness and fatigue crack paths in such cases. Such mixed-mode problems involve crack orientation and/or load conditions that lead to combined local Stress Intensity Factors (SIFs) K_I-K_{II} around the crack front. Therefore, it is almost a truism to claim that analyses of cracked components that induce mixed-mode conditions around the crack tip under multiaxial stress states are needed to properly evaluate their fatigue and fracture behavior.

It is well known that geometric parameters, loading conditions, and transversal constraints can affect plastic zone (*pz*) sizes and shapes. Indeed, for instance under pure mode I conditions, a given SIF value K_I can provide different *pz* sizes and shapes in thin or thick components, due to dominant plane stress or plane strain conditions along the crack front. This effect is due to transversal displacement constraints around the crack tip in thick components, which may restrict the *pz* formation by inducing higher localized hydrostatic stress components (in comparison to the prevalent conditions in thin plane stress cracked components). In the case of pure mode I loadings, there is a number of detailed 3D numerical studies to quantify *pz* effects on the structural integrity of cracked mechanical components [1–4].

However, what is certainly less well-known is that *pz* sizes and shapes can be much affected as well by equally important nominal load and crack size effects, which make *pz*s much dependent on σ_n/S_Y and a/W ratios. Such effects are simply neglected in traditional *pz* estimates, which assume *pz* sizes and shapes depend only on the SIFs and on the cracked component thickness, even though relatively simple improved estimates can clearly identify non-negligible σ_n/S_Y effects [5]. Therefore, it should not be a surprise that traditional *pz* estimates, as well as

* Corresponding author.
E-mail addresses: lfernando@unifesspa.edu.br (L.F.N. Marques), meggi@puc-rio.br (M.A. Meggiolaro), jtcastro@puc-rio.br (J.T.P.d. Castro), lfm@tecgraf.puc-rio.br (L.F. Martha).

https://doi.org/10.1016/j.tafmec.2020.102490
Received 29 October 2019; Received in revised form 13 December 2019; Accepted 12 January 2020
Available online 17 February 2020

Nomenclature

a	crack length
B	specimen thickness
E	Young's modulus of elasticity
EP	elastoplastic
E_s	element size
FE	finite element
f_i, g_i	geometry factors
H	monotonic Ramberg-Osgood hardening coefficient
h	monotonic Ramberg-Osgood hardening exponent
J	J-integral (energy release rate of EP materials)
J_{IC}	plane strain fracture toughness characterized by J
K, K_I	stress intensity factor (SIF) in mode I
K_{eq}	equivalent SIF
K_{IC}	plane strain fracture toughness
K_{II}	SIF in mode II
L	half-height of SE(T)
LE	linear elastic
mp	middle position
P	load
pl, PL	plastic
pl-ε	plane strain
pl-σ	plane stress
pz	plastic zone
SE(T)	single edge tension specimen
SIF	stress concentration factor
S_Y	yield strength
T_z	transversal constraint factor
$u(x)$	horizontal displacement
U_{ep}	elastoplastic work
u_{ep}	elastoplastic work density
U_{pl}	plastic work
$v(y)$	vertical displacement
V_e	volume of the element
V_{pz}	plastic zone volume
W	specimen width
$w(z)$	out-of-plane displacement
x, y, z	global Cartesian coordinates
ν	Poisson's coefficient
σ_n	nominal stress
δ_{IC}	critical crack tip opening displacement
ε_{eq}	von Mises equivalent strain
ε_Y	yield strain
β	crack inclination angle

structural integrity evaluations based on idealized SIF-dominated stress/strain fields, can be highly inaccurate and even useless for many practical applications where reliable predictions are needed.

Moreover, probably due to the widespread use of traditional SIF-based pz estimates, σ_n/S_Y and a/W effects are not properly evaluated or even considered in many numerical studies either. To show how inappropriate this practice can be, a recent work [6] used extensive 3D incremental elastoplastic (EP) numerical simulations to calculate the plastic work U_{pl} dissipated inside the pz under a given K_I value, but different σ_n/S_Y and a/W conditions. That work quantitatively evaluates the use of U_{pl} to estimate the onset of crack tearing in practical EP fracture applications, and presents some experimental evidence to support the use of this simple idea. Such σ_n/S_Y and a/W effects can explain the typically high dispersion of EP fracture toughness measurements in non-identical specimens. Indeed, from a physical point of view, the toughness should be controlled by U_{pl} in most practical applications, since the work spent to create two new crack faces is usually negligible in tough materials.

In fact, if the plastic zone sizes and shapes ahead of crack tips, and thus the pz volumes and the U_{pl}spent inside them, strongly depend on geometric parameters, loading conditions, and transversal constraints, the consequent toughness should depend on σ_n/S_Y and a/W *ratios* as well. This U_{pl}-dependent toughness may become a practical tool to replace too conservative toughness estimates for design purposes based on highly constrained K [7] or J [8] measurements [4,9–11]. Indeed, a recent contribution discusses a methodology to obtain results of strain measurements using synchrotron X-ray diffraction [11], which are compared with those predicted from 3D EP FEM. This kind of experimental work may also be useful to quantify the dependence of fracture toughness on the 3D plastic constraint.

Standards for toughness measurements [7,8] are available only for pure mode I, which can be highly conservative in many mixed-mode design cases. A recent work [12] shows through numerical and analytical calculations that the classic estimates for the pz size of shear-mode cracks must be corrected. Based on a comparison between linear elastic fracture mechanics (LEFM), the HRR field [13] and FEM, the correct assessment of the pzs must be carefully performed because part of the applied load is transferred by fracture surfaces. Another recent contribution presents numerical analyses and correlations between the plastic SIF and the constraint parameter for a range of mixed-mode loadings [14].

It is reasonable to extend to mixed mode I-II problems the idea that U_{pl} can and (at least in the authors' opinion) should be used to quantify EP toughness in practical applications, in particular because its numerical calculation by EP finite element procedures (although not a trivial task) is not anymore a major barrier nowadays.

In this work, single edge tension (SE(T)) specimens are numerically investigated to evaluate 3D crack tip plastic zones for several values of equivalent SIF K_{eq}, crack inclination angle β, W/B width-to-thickness ratio, and a/W crack length-to-specimen width ratio, for mixed mode I–II problems. Moreover, to validate the used numerical models, they are compared to experimental photoelastic tests and 2D numerical studies under mixed mode I–II configurations, which have been previously examined and well documented elsewhere [16–18].

This work describes and uses an improved methodology for evaluating 3D pz volumes around crack fronts, based on 3D elastoplastic (EP) submodeling finite element (FE) techniques proposed and detailed elsewhere [6]. This methodology can be used to evaluate cracked components under different transversal constraint levels. These constraints are varied changing the specimen geometry and loading conditions. Geometric parameters are represented by crack length-to-specimen width a/W and specimen width-to-specimen thickness W/B ratios. Loading conditions are considered by examining different nominal stress-to-yield strength σ_n/S_Y ratios for a given K_I or combined K_I-K_{II}, which can also be represented as K_{eq} or $K_{eq}^2 = K_I^2 + K_{II}^2$.

In the following Sections, 3D EP FE models are used to calculate several pz sizes and shapes in cracked specimens, their pz volumes, as well as the corresponding plastic work spent U_{pl} inside them. Different transversal displacement constraints around the crack front are considered, under various K_{eq}, β, a/W and W/B ratios. Multiaxial loading conditions are analyzed by varying the crack inclination angle β in a modified mixed-mode K_I-K_{II} single edge tension SE(T) specimen [17], as illustrated in Fig. 1, where the specimen width is W, its height is $2L$, its thickness is B, and the crack length is a.

2. Finite element analysis

A modified SE(T) specimen is considered in this study to simulate mixed mode I–II loading conditions by simply varying the crack angle β, as depicted in Fig. 1. Pure mode I loading conditions are achieved when

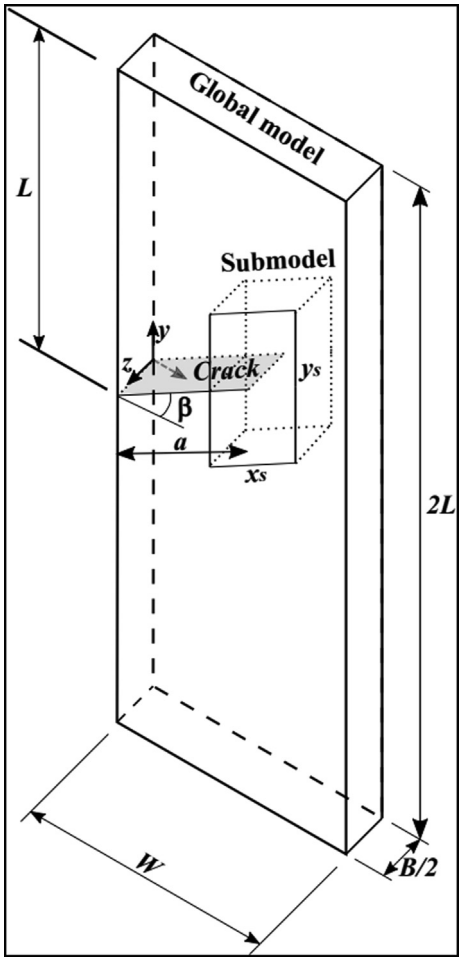

Fig. 1. Some characteristics of the global models and sub-models used to analyze mixed mode I–II single edge tension SE(T) specimens.

$\beta = 0°$. This modified SE(T) specimen is supposed to carry a purely tensile nominal stress σ_n at its upper extremity ($y = L$), assuming a uniformly distributed load P per unit area $W{\cdot}B$ in the y-axis direction. The lower SE(T) extremity ($y = -L$) is assumed fixed in all degrees of freedom.

First, the submodel loading conditions are obtained from the numerical solution of the global model, using proper elements to globally describe its crack. The submodel sizes (x_s, y_x, $B/2$) are then chosen to assure LE conditions all around its perimeter, keeping the *pz* inside the submodel. All numerical finite element (FE) calculations are performed considering (in the submodel) its symmetry about the *xy*-plane (*z*-axis). When $\beta = 0°$, only 1/4 of the specimen needs to be modeled, due to the additional symmetry in the *xz*-plane (*y*-axis). Then, refined 3D EP FE calculations are performed in the submodel to obtain the desired *pz* volumes as well as the plastic work U_{pl} performed inside them. To do so, the Ansys Parametric Design Language (APDL) is used. Further details about the numerical problem can be found in [6], which focuses only on pure mode I.

The properties of the material used in all simulations are presented in Table 1 [15,19], where E is Young's modulus, ν is Poisson's coefficient, S_Y is the yielding strength, and H and h are the monotonic Ramberg-Osgood strain hardening coefficient and exponent.

2.1. FE model

The FE procedure involves two calculation steps. First, the global model with a relatively coarse mesh is numerically solved to quantify the stress field inside it, considering the inclined crack effect. This requires the use of proper elements to simulate the crack tip behavior, but besides this precaution it poses no major problems. Then, a submodel that contains the crack tip and its entire *pz* volume is chosen for mesh refination purposes, assuring LE conditions around its perimeter in the global model, which are used as displacement loading conditions for such a submodel. This submodel is remeshed to assure that the required accuracy can be achieved when numerically solving its EP stress/strain fields.

The *pz* 3D EP frontiers are mapped in terms of the equivalent von Mises strain ε_{eq}. Quadratic elements (3D SOLID186) are used in these FE simulations, and only the fractions of the volumes corresponding to their plastified Gauss integration points are counted as part of the 3D *pz* around the crack fronts ($\varepsilon_{eq} \geq \varepsilon_Y$). Hence, the smallest unit of volume considered in the *pz* models, and in the calculation of the plastic work U_{pl} performed inside them, becomes 1/8 of the total volume of the element [6].

When this modified SE(T) specimen with an inclined crack (which provides mixed mode I–II conditions simply by varying its crack inclination angle β) is large and its residual ligament is much larger than its crack size, then there are well-known, easy-to-deduce analytical expressions for its SIFs K_I and K_{II}. When the modified SE(T) residual ligament is not much larger than a, see e.g. [18], the general expression for its K_i is given by [18]:

$$K_i = \sigma_n \sqrt{a} \cdot f_i \cdot g_i \tag{1}$$

where σ_n is the nominal tensile stress applied in the cracked specimen upper boundary ($y = L$), see Fig. 1, and f_i and g_i are geometry factors that depend on the crack size-to-specimen width a/W ratio and on α_i, δ_i, and γ_i parameters defined below, with i = I or II, namely:

$$g_I = \cos^2\beta \tag{2}$$

$$g_{II} = \cos\beta \sin\beta \tag{3}$$

$$f_i(a/W, \alpha_i, \delta_i, \gamma_i) = \gamma_i \cdot [\cos(a/W)]^{-\delta_i} + \alpha_i \cdot (a/W) \tag{4}$$

$$\alpha_I = 1.12/[\beta^3 - 0.73\beta^2 + 0.8] \tag{5}$$

$$\delta_I = [8.53 - 5.57\beta]/[\beta^2 - 0.82\beta + 1.37] \tag{6}$$

$$\gamma_I = 1.9 \cdot (\cos\beta)^{-0.921} - 0.38\beta^{2.03} \tag{7}$$

$$\alpha_{II} = 0.8\beta^3 - 2.53\beta^2 + 1.66\beta + 0.54 \tag{8}$$

$$\delta_{II} = 2.85\beta^3 - 6.4\beta^2 + 5.1 \tag{9}$$

$$\gamma_{II} = 1.2 \cdot (\cos\beta)^{-0.3} - 0.15\beta \tag{10}$$

The geometric parameters and SIFs used in this work under modes I and II, see Eq. (1), are presented in Tables 2 and 3, where $W = 50$ mm and $L = 2\,W$. Six values for the crack inclination angle β are considered: 0° (pure mode I), 20°, 40°, 50°, 55°, and 60°. Six a/W ratios are examined as well, namely 0.2, 0.3, 0.4, 0.5, 0.6, and 0.7. Three equivalent SIF K_{eq} are also studied, 10, 50 and 100 MPa√m, as well as three W/B ratios, 2, 4, and 6.25.

Before all submodel simulations, a study of compatibility conditions between the global model and submodel is performed. In addition, a mesh convergence study is also carried out, based on evaluations of the *pz* volume V_{pz}.

Table 1
Materials and properties [19].

Material	E (GPa)	ν (–)	S_Y (MPa)	H (MPa)	h (–)
API 5L X80	207	0.3	560	892	0.08

Table 2
Evaluated cases for K_{eq} = 100 MPa√m, and W/B = 6.25.

β (°)	a/W = 0.2				a/W = 0.3			
	K_I (MPa√m)	K_{II} (MPa√m)	K_{II}/K_I (–)	σ_n/S_Y (–)	K_I (MPa√m)	K_{II} (MPa√m)	K_{II}/K_I (–)	σ_n/S_Y (–)
0	100	0	0	0.73	100	0	0	0.50
20	98	18	0.19	0.71	98	18	0.19	0.49
40	96	28	0.29	0.72	96	28	0.29	0.52
50	95	31	0.33	0.79	95	31	0.33	0.59
55	94	33	0.35	0.88	95	33	0.35	0.66
60	93	36	0.39	1.04	93	36	0.39	0.80
	a/W = 0.4				a/W = 0.5			
0	100	0	0	0.34	100	0	0	0.23
20	99	18	0.19	0.34	99	17	0.17	0.24
40	97	27	0.28	0.38	97	27	0.27	0.27
50	95	30	0.32	0.45	96	30	0.31	0.35
55	95	32	0.34	0.52	95	32	0.34	0.41
60	94	36	0.39	0.64	93	36	0.38	0.52
	a/W = 0.6				a/W = 0.7			
0	100	0	0	0.14	100	0	0	0.09
20	99	16	0.16	0.16	99	15	0.15	0.10
40	97	26	0.26	0.21	97	25	0.25	0.15
50	96	29	0.30	0.27	96	28	0.29	0.21
55	95	31	0.33	0.33	95	31	0.33	0.26
60	94	35	0.37	0.42	94	34	0.37	0.35

2.2. Compatibility and convergence studies

As the FE calculations involve two-step solutions (first a global model and then a submodel), to assure their compatibility and convergence it is necessary to find how (coarse/refined) the FE mesh should be in the (global/sub) model. The appropriate mesh size must present geometric and stress compatibilities between both the global model and the submodel. To do so, three kinds of analyses are performed. First, both models are solved using 3D LE FE. Second, the global model is solved with 3D LE FE and then its submodel is solved with 3D EP FE. Finally, both models are solved with 3D EP FE, a computationally costly procedure just to verify the quality of the results from the efficient submodeling technique. All these analyses are performed considering the values K_{eq} = 100 MPa√m, β = 0° (pure mode I), a/W = 0.5, W/B = 2 and σ_n/S_Y = 0.23. The results are presented in terms of plastic zone volume V_{pz} (Fig. 2), as well as vertical $v(y)$ and transversal $w(z)$ displacements along the crack plane (y = 0) on the surface of the specimen (z = $B/2$), see Figs. 3 and 4, respectively.

Fig. 2 shows that V_{pz} depends on the element type/size, as is reported elsewhere [6]. Likewise, it depends on the kind of analysis performed in this work. For instance, the LE global model with four elements along the modeled half-thickness $B/2$, combined with the EP submodel with thirty elements along its half-thickness (G4/S30-LE/EP), shows V_{pz} converging to 148 mm^3. The G4/S30-LE/LE model converges this V_{pz} to 182 mm^3, while the G4/S30-EP/EP converges to 326 mm^3, a huge difference between them. However, the V_{pz} on these three models converges using at least 15–20 elements along $B/2$, as is reported in [6].

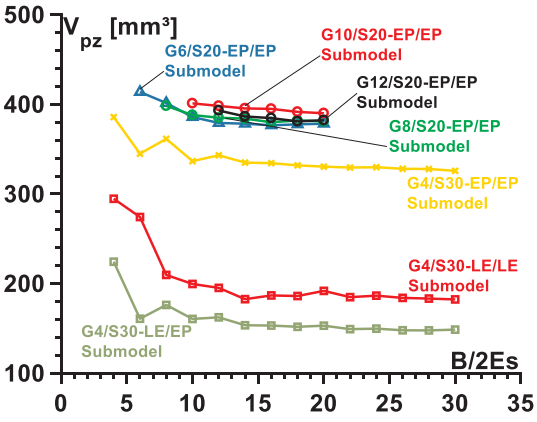

Fig. 2. Analysis of V_{pz} for 7 different cases.

When the number of elements on the global model increases to 6, 8, 10 and 12, the V_{pz} converges to a value between 380 and 390 mm^3. Hence, these results suggest that the best model to be used in other simulations is the G6/S20-EP/EP.

Fig. 3 shows the vertical displacement results for five different cases. The displacement of the crack face is more pronounced when both models use EP FE analyses. The results of the global model with six elements along $B/2$ are also included. The same trend is noted when the transversal displacement is evaluated in Fig. 4.

Finally, Fig. 5 presents the evaluation of the transversal constraint

Table 3
Evaluated cases for W/B = 6.25 and a/W = 0.2.

β (°)	K_{eq} = 10 MPa√m			K_{eq} = 50 MPa√m		
	K_I (MPa√m)	K_{II} (MPa√m)	σ_n/S_Y (–)	K_I (MPa√m)	K_{II} (MPa√m)	σ_n/S_Y (–)
0	10	0	0.07	50	0	0.36
20	9.8	1.8	0.07	49	9	0.35
40	9.6	2.8	0.07	48	14	0.36
50	9.5	3.1	0.08	47	15	0.39
55	9.4	3.3	0.09	47	16	0.44
60	9.3	3.6	0.10	46	18	0.52

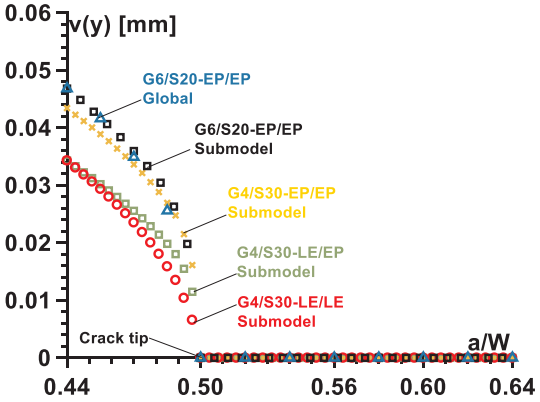

Fig. 3. Numerical vertical displacement ($v(y)$) fields at the crack plane.

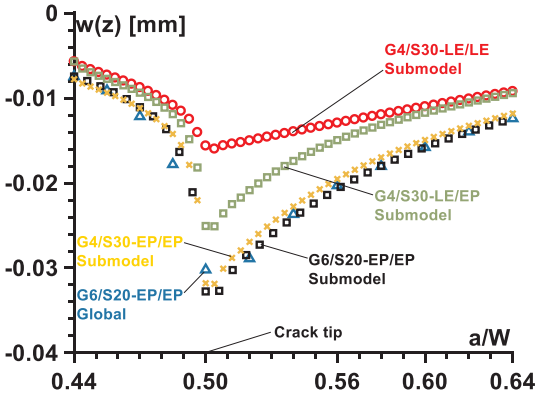

Fig. 4. Numerical transversal displacement ($w(z)$) fields at the crack plane.

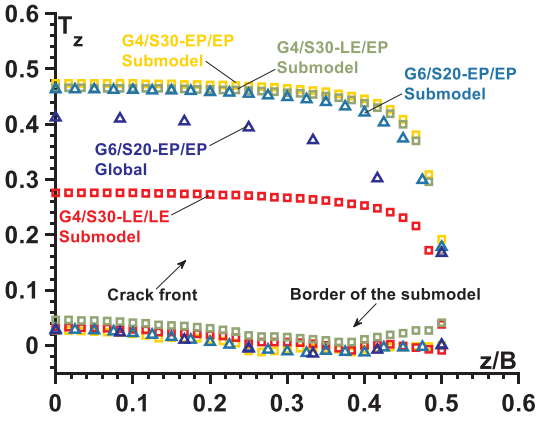

Fig. 5. Transversal constraint factor distribution along the crack front (x = a/W) and along the rear border of the submodel, both on the crack plane ($y = 0$).

factor T_z, defined by the ratio between the transversal stress σ_z and the sum of the two in-plane stress components σ_x and σ_y, namely $T_z = \sigma_z/(\sigma_x + \sigma_y)$. Fig. 5 shows T_z along the crack front and along the rear border of the submodel for 5 different cases. The constraint factor T_z gradually decreases from its maximum value ($T_z \rightarrow \nu$) at the plate mid-plane ($z/B = 0$) to $T_z = 0$ on the free surface. All submodels analyzed by EP FE present T_z near $\nu = 0.5$ at the mid-plane. When the submodel is evaluated by LE FE, the constraint factor T_z is slightly below $\nu = 0.3$. The global model analyzed by EP FE presents an intermediate value of 0.4. To maintain compatibility between the global model and the submodel, the sizes of the last one must be chosen so that the T_z distribution along the thickness is near zero on its border, as reported elsewhere [20]. These results show that compatibility is achieved for all submodels.

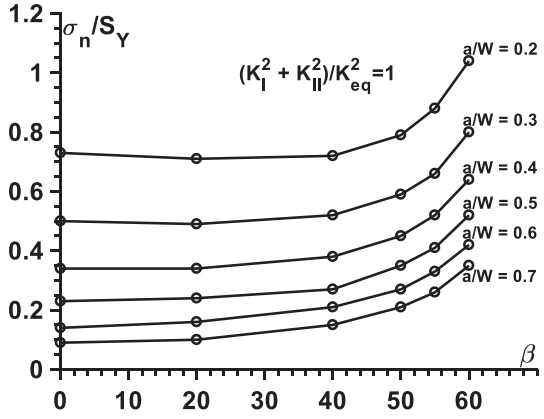

Fig. 6. Analysis of the σ_n/S_Y ratio for $K_{eq} = 100$ MPa√m.

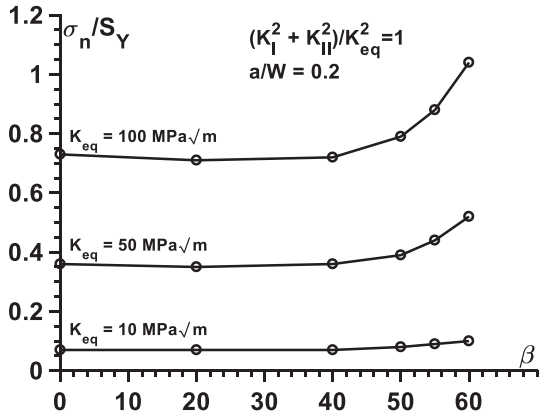

Fig. 7. Analysis of the σ_n/S_Y ratio for $a/W = 0.2$.

3. Numerical results for differently constrained specimens

To evaluate differently constrained specimens along the crack front, calculations using different σ_n/S_Y ratios are performed for a given value of K_{eq}, see Figs. 6 and 7, where $K_{eq}^2 = K_I^2 + K_{II}^2$. As it can be seen in the figures, when the crack angle β increases for each crack size-to-width ratio a/W, the σ_n/S_Y ratio also increases. However, the σ_n/S_Y ratio decreases for long cracks a/W and low values of K_{eq}. These analyses are performed considering the cases presented in Tables 2 and 3. An increase of the σ_n/S_Y ratio induces large volumes V_{pz} of plastic zones ahead of the crack front, as discussed elsewhere [6].

Table 4 summarizes the shapes and sizes of the EP pz frontiers numerically calculated on the surface of the modified SE(T), considering the properties listed in Table 1 and some cases presented in Table 2. Plastic zone frontiers are evaluated for $W/B = 6.25$ and $K_{eq} = 100$ MPa√m, a value well below the toughness of the API 5L X80 steel, so they can be directly compared without any crack tearing concern. Note that the ratio σ_n/S_Y and the volume V_{pz} vary significantly between crack inclination angles 40° and 60°. The EP pz frontiers are properly scaled to allow the direct comparison among the various cases that have the same a/W. Table 5 shows V_{pz} and U_{pl} values calculated using 3D EP EF for both global models and submodels, to avoid any eventual numerical error from an elastic analysis of the global model. Figs. 8–11 show the calculated V_{pz} and U_{pl} for several β and K_{eq} values.

As the fracture resistance depends on geometric parameters, loading conditions, and transversal constraints, which much affect pz sizes and shapes, so does the U_{pl} spent inside the pz. The results presented in this paper reinforce the idea that the ratios σ_n/S_Y and a/W can much affect the plastic zones sizes and shapes, as well as the plastic work U_{pl} dissipated inside them. Since it is reasonable to assume that the toughness of most metallic cracked structural components primarily depends on

Table 4
Shape and size of the *pz* on the surface of the specimen.

β (°)\a/W	0.3	0.4	0.5	0.6	0.7
0					
20					
40					
60					

the U_{pl} spent inside the *pz*, a proposal to validate the 3D EP FE calculations through suitable fracture toughness measurements has been published elsewhere [6]. This idea states that the ratio of fracture toughness measured at the threshold of crack tearing for different constraint levels ($J_{IC,\sigma\text{-}pl}/J_{IC,\varepsilon\text{-}pl}$ or $\delta_{IC,\sigma\text{-}pl}/\delta_{IC,\varepsilon\text{-}pl}$) could be correlated with the ratio of the values of plastic work per *pz* volumes (U_{pl}/V_{pz}) developed around crack fronts. In other words, it is suggested that EP fracture toughness should be controlled by V_{pz} and U_{pl}. Experimental fracture toughness under mixed-mode K_I-K_{II} conditions should be measured in future works to extend this idea to multiaxial loadings.

Figs. 12–14 present the predicted variation of U_{pl}/V_{pz} for different geometries (a/W, W/B and β) and load (K_{eq} and σ_n/S_Y) combinations. For the smallest thickness B ($W/B = 6.25$), Fig. 12 shows that the parameter U_{pl}/V_{pz} behaves like the parameters V_{pz} and U_{pl} when analyzed separately (see Figs. 10 and 11). In these cases, all evaluated parameters are maximized at $\beta = 60^\circ$. However, for larger thicknesses ($W/B = 2$), the parameter U_{pl}/V_{pz} is maximized at $\beta = 40^\circ$ for $K_{eq} = 100$ MPa√m and $a/W = 0.7$. Figs. 13 and 14 show the behavior of the parameter U_{pl}/V_{pz} as a function of a/W and K_{eq}, respectively.

Finally, Fig. 15 shows details of the plastic zone around the crack front for $K_{eq} = 100$ MPa√m, $\beta = 50^\circ$, $a/W = 0.6$, $W/B = 2$ and $\sigma_n/S_Y = 0.27$. It can be seen that the plastic zone size and shape vary along the specimen thickness (*z*-axis) from the surface to the mid-plane. Note, however, that the maximum width of the plastic zone (size along the *x* direction) is found in the interior of the specimen, closer to the surface than to the mid plane. The same behavior was observed in other works for mode I [1,2,21]. Note that this behavior depends on the thickness of the specimen.

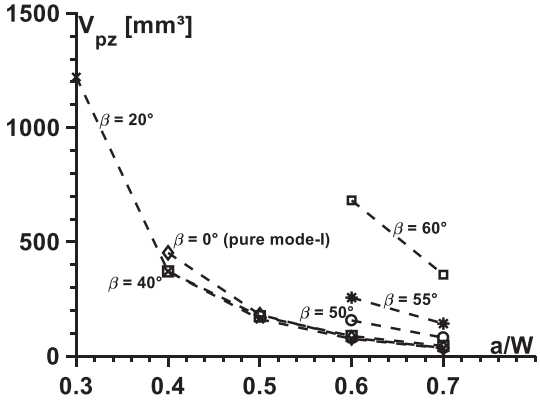

Fig. 8. Plastic zone volumes V_{pz} for $K_{eq} = 100$ MPa√m and $W/B = 6.25$.

4. Conclusions

Three-dimensional elastic and elastoplastic finite element analyses have been performed to generate numerical predictions of plastic zone sizes, shapes, frontiers and volumes in modified cracked SE(T) specimens under standard pure mode I (crack inclination angle $\beta = 0^\circ$) and under mixed mode I–II ($\beta > 0^\circ$). Validations based on displacements and transversal constraint factors show that compatibilities are

Table 5
Plastic zone volumes V_{pz} and plastic work U_{pl} for $K_{eq} = 100$ MPa√m and $W/B = 6.25$.

β (°)	$a/W = 0.2$		$a/W = 0.3$		$a/W = 0.4$		$a/W = 0.5$	$a/W = 0.6$	$a/W = 0.7$
	V_{pz} (mm³)	U_{pl} (mJ)	V_{pz} (mm³)	U_{pl} (mJ)	V_{pz} (mm³)	U_{pl} (mJ)	V_{pz} (mm³)	U_{pl} (mJ)	V_{pz} (mm³)
0	–	–	–	–	452.12	525.21	181.47	177.07	79.95
20	–	–	1221.05	1384.06	370.79	460.59	161.78	152.64	75.76
40	–	–	–	–	370.75	389.03	174.60	165.22	88.05
50	–	–	–	–	–	–	–	–	155.98
55	–	–	–	–	–	–	–	–	256.04
60	–	–	–	–	–	–	–	–	681.70

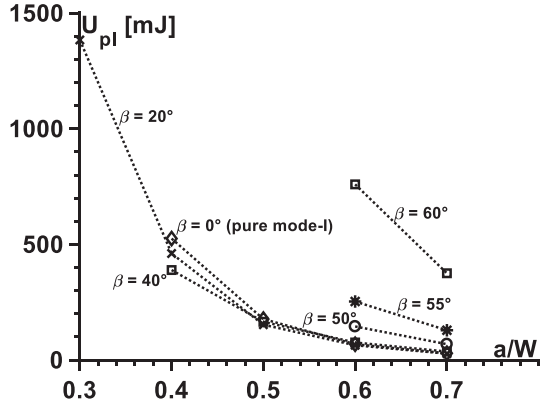

Fig. 9. Plastic work U_{pl} for K_{eq} = 100 MPa√m and W/B = 6.25.

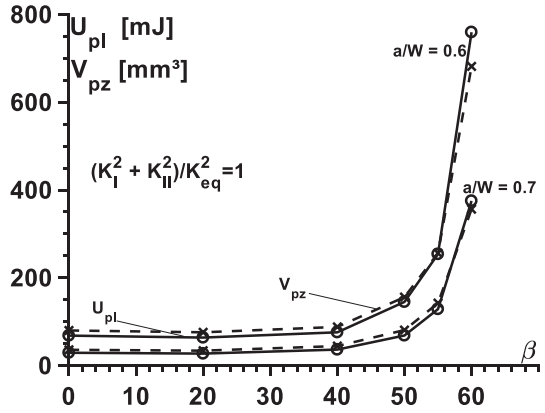

Fig. 10. Plastic zone volumes V_{pz} and plastic work U_{pl} for K_{eq} = 100 MPa√m, W/B = 6.25 and different crack length ratios a/W.

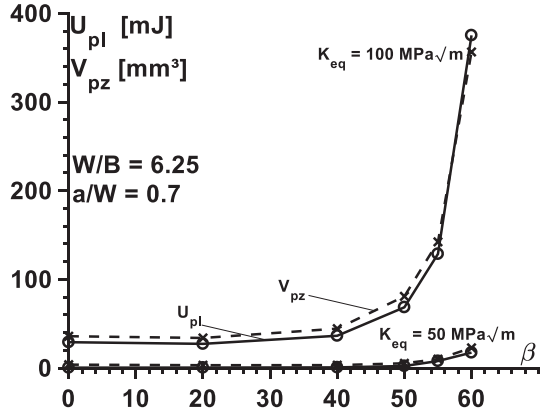

Fig. 11. Plastic zone volumes V_{pz} and plastic work U_{pl} for a/W = 0.7, W/B = 6.25 and different equivalent SIFs K_{eq}.

achieved between global FE models and submodels. For a given equivalent stress intensity factor ${K_{eq}}^2 = {K_I}^2 + {K_{II}}^2$, as the crack inclination angle β increases, the plastic zone size increases and becomes non-symmetrical about the crack length/front. The variations of the ratio σ_n/S_Y and of the plastic zone volume V_{pz} are significant between crack inclination angles 40° and 60°. Moreover, the plastic zone size is much affected by the nominal stress-to-yield strength σ_n/S_Y ratio, and decreases while increasing the crack length-to-width ratio a/W. The presented calculations of plastic zone sizes and shapes, as well as the associated plastic work dissipated inside them, can be useful for fatigue and fracture mechanics assessments, not to mention fracture toughness evaluations, replacing unreliable combinations based solely on K or J

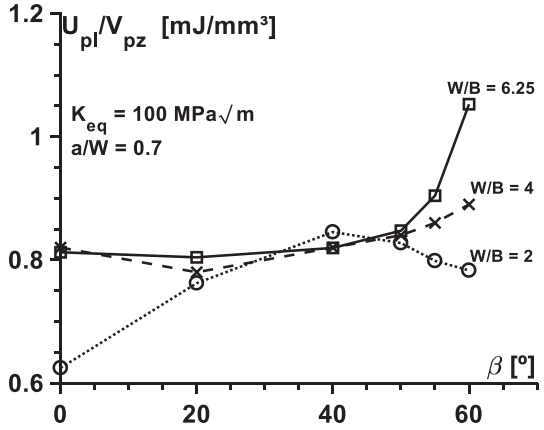

Fig. 12. Plastic work per pz volume for some β values and three conditions of thicknesses.

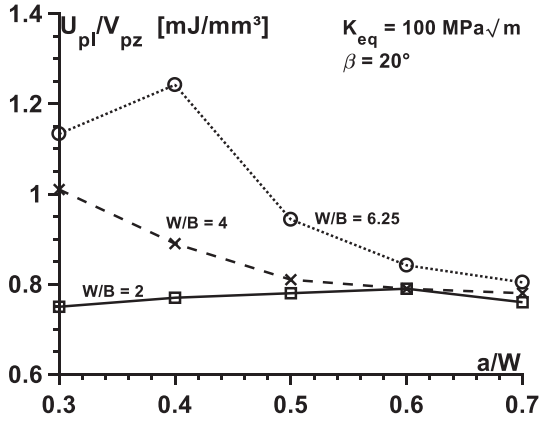

Fig. 13. Plastic work per pz volume for some crack length values and three thickness conditions.

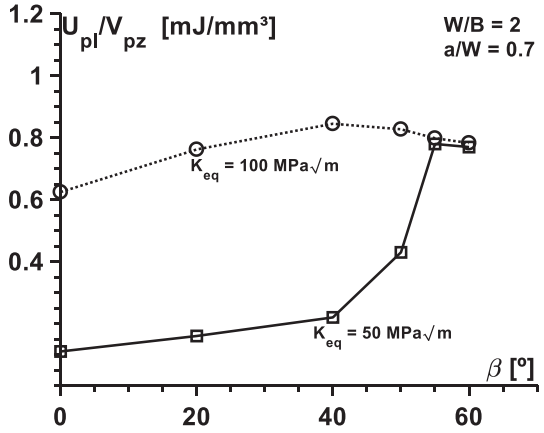

Fig. 14. Plastic work per pz volume for β values and two equivalent SIFs.

and even on their combinations with T-stress-like constraint parameters.

CRediT authorship contribution statement

Luiz Fernando Nazaré Marques: Methodology, Software, Validation, Writing - original draft. **Marco Antonio Meggiolaro:** Methodology, Supervision, Writing - review & editing. **Jaime Tupiassú Pinho de Castro:** Conceptualization, Methodology, Writing - review & editing. **Luiz Fernando Martha:** Methodology, Writing - review &

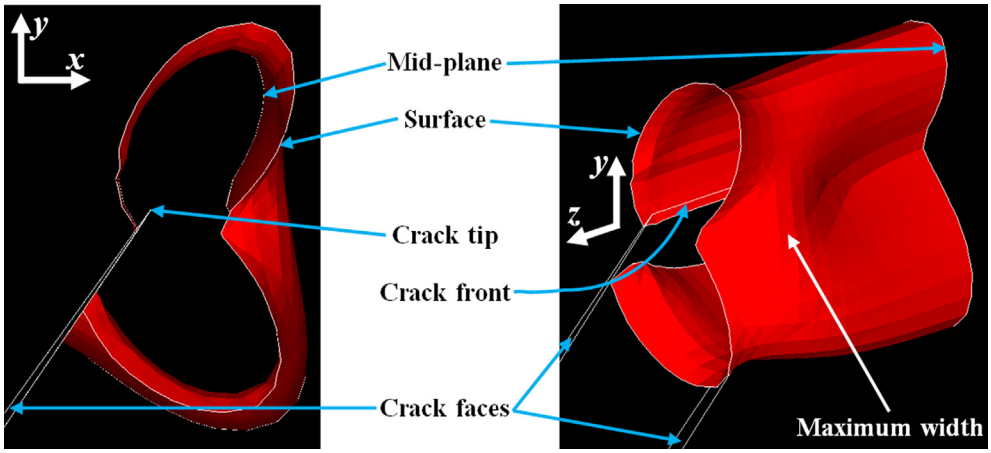

Fig. 15. Plastic zone shape variation along its thickness, showing the region where its width is maximized.

editing.

Declaration of Competing Interest

The authors declare that they have no known competing financial interests or personal relationships that could have appeared to influence the work reported in this paper.

Acknowledgement

The authors would like to thank the Brazilian funding agency CAPES for the scholarships granted.

References

[1] M. Besel, E. Breitbarth, Advanced analysis of crack tip plastic zone under cyclic loading, Int. J. Fatigue 93 (2016) 92–108.
[2] D. Camas, J. Garcia-Manrique, A. Gonzalez-Herrera, Numerical study of the thickness transition in bi-dimensional specimen cracks, Int. J. Fatigue 33 (2011) 921–928.
[3] D. Camas, et al., Numerical and experimental study of the plastic zone in cracked specimens, Eng. Fract. Mech. 185 (2017) 20–32.
[4] F. Yusof, Three-dimensional assessments of crack tip constraint, Theor. Appl. Fract. Mech. (2019), https://doi.org/10.1016/j.tafmec.2019.01.025.
[5] R.A. Souza, J.T.P. Castro, A.A.O. Lopes, L.F. Martha, On improved crack tip plastic zone estimates based on T-stress and on complete stress fields, Fatigue Fract. Eng. Mater. Struct. 36 (2013) 25–38.
[6] L.F.N. Marques, E.E. Cota, J.T.P. Castro, L.F. Martha, M.A. Meggiolaro, On the estimation of the elastoplastic work needed to initiate crack tearing, Theor. Appl. Fract. Mech. 101 (2019) 80–91.
[7] ASTM E399-12, Standard test method for linear-elastic plane-strain fracture toughness KIC of metallic materials, American Society for Testing and Materials, 2018.
[8] ASTM E1820-17a, Standard test method for measurement of fracture toughness, American Society for Testing and Materials, 2018.
[9] T. Kawabata, et al., Investigation on η and m factors for J integral in SE(B) specimens, Theor. Appl. Fract. Mech. 97 (2018) 224–235.
[10] D. Sen, J. Chattopadhyay, New η-factor equation for evaluation of J-integral of shallow cracked CT specimen considering R-O material strain hardening, Theor. Appl. Fract. Mech. 97 (2018) 98–107.
[11] C.A. Simpson, et al., Validating 3D two-parameter fracture mechanics models for structural integrity assessments, Theor. Appl. Fract. Mech. (2019), https://doi.org/10.1016/j.tafmec.2019.102281.
[12] T. Vojtek, M. Hrstka, How to get a correct estimate of the plastic zone size for shear-mode fatigue cracks? Theor. Appl. Fract. Mech. (2019), https://doi.org/10.1016/j.tafmec.2019.102332.
[13] J.W. Hutchinson, Singular behavior at the end of a tensile crack in a hardening material, J. Mech. Phys. Solids 16 (1968) 13–31.
[14] V.N. Shlyannikov, A.P. Zakharov, Generalization of mixed mode crack behaviour by the plastic stress intensity factor, Theor. Appl. Fract. Mech. (2017), https://doi.org/10.1016/j.tafmec.2017.03.014.
[15] S.M.A. Khan, N. Merah, M.J. Adinoyi, 3D effects on crack front core regions, stress intensity factors and crack initiation angles, Int. J. Solids Struct 50 (2013) 1449–1459.
[16] W.K. Wilson, On Combined Mode Fracture Mechanics, Research report 69–1E7-FMECH-R1, Westinghouse Research Laboratories, Pittsburgh, 1969.
[17] N. Merah, J. Albinmousa, Experimental and numerical determination of mixed mode extension angle, ASTM J. Test Eval. 37 (2008) 95–107.
[18] J. Albinmousa, et al., A model for calculating geometry factors for a mixed-mode I-II single edge notched tension specimen, Eng. Fract. Mech. 78 (2011) 3300–3307.
[19] G. Shen, W.R. Tyson, A. Glover, D. Horsley, Constraint effects on pipeline toughness, Proc. 4th Int Conf. Pipeline Tech. vol. 2, 2004, pp. 703–720.
[20] R.C.O. Góes, J.T.P. Castro, L.F. Martha, 3D effects around notch and crack tips, Int. J. Fatigue 62 (2014) 159–170.
[21] P. Lopez-Crespo, D. Camas, F.V. Antunes, J.R. Yates, A study of the evolution of crack tip plasticity along a crack front, Theor. Appl. Fract. Mech. (2018), https://doi.org/10.1016/j.tafmec.2018.09.012.